Effective segmentation of fresh *post-mortem* murine lung parenchyma in phase contrast X-ray tomographic microscopy images

IOP Conf. Series: Journal of Physics: Conf. Series **849** (2017) 012006 doi:10.1088/1742-6596/849/1/012006

Effective segmentation of fresh *post-mortem* murine lung parenchyma in phase contrast X-ray tomographic microscopy images

Ioannis Vogiatzis Oikonomidis[1,2], Tiziana P Cremona[1], Goran Lovric[2,3], Filippo Arcadu[2,4], Marco Stampanoni[2,4] and Johannes C Schittny[1]

[1] Institute of Anatomy, University of Bern, 3012 Bern, Switzerland
[2] Swiss Light Source, Paul Scherrer Institute, 5234 Villigen, Switzerland
[3] Center for Biomedical Imaging (CIBM), EPFL, 1015 Lausanne, Switzerland
[4] Institute for Biomedical Engineering, University and ETH Zurich, 8092 Zurich, Switzerland

E-mail: ioannis.vogiatzis@ana.unibe.ch

Abstract. The acinus represents the functional unit of the mammalian lung. It is defined as the small tree of gas-exchanging airways, which is fed by the most distal purely conducting airway. Different hypotheses exist on how the fine structure of the acinus changes during ventilation and development. Since in classical 2-dimensional (2D) sections of the lung the borders of the acini are not detectable, every study of acini requires 3-dimensional (3D) datasets. As a basis for further studies of pulmonary acini we imaged rodent lungs as close to life as possible using phase contrast synchrotron radiation-based X-ray tomographic microscopy (SRXTM), and developed a protocol for the segmentation of the alveolar septa. The method is based on a combined multilevel filtering approach. Seeds are automatically defined for separate regions of tissue and airspace during each 2D filtering level and then given as input to a 3D random walk segmentation. Thus, the different types of artifacts present in the images are treated separately, taking into account the sample's structural complexity. The proposed procedure yields high-quality 3D segmentations of acinar microstructure that can be used for a reliable morphological analysis.

1. Introduction

The mammalian lung is a vital organ facilitating the gas-exchange between the ambient air and the blood. The gas-exchange area consists of functional units called acini which represent small trees of gas-exchanging airways. There is limited knowledge about the 3D microscopic dynamics and development of the acini, because their borders may not be recognized in classical 2D-sections. Therefore, the link between microscopic observations and specific lung function is still incomplete. Furthermore, the connection between lung diseases and the changes in the acinar microstructure is not fully understood.

3D imaging and morphological quantifications have become essential to further understand the function and development of the lung and in addressing the questions outlined above. The imaging setup needs to feature sufficient temporal and spatial resolution to correctly segment and recognize the acinus.

Here, we introduce an automatic segmentation method that can correctly differentiate the thin septa between the borders of small alveoli from air. Our technique is based on a combined multilevel filtering approach that takes into account the complex 3D structure of the lung. The method offers an unsupervised platform for the automatic extraction of the skeleton of the alveolar septa, which is essential for analyzing the deformation of inflated lungs as well as to track their development.

2. Materials and Methods

2.1. Image Acquisition, Animal Preparation and CT-reconstructions

Data were acquired at the X02DA TOMCAT beamline of the Swiss Light Source (SLS) at the Paul Scherrer Institute (Villigen, Switzerland). The experimental setup is illustrated in detail in [1]. A sample-to-source distance of $25\,m$ at $21\,keV$ was chosen as a good trade-off between contrast-to-noise ratio (CNR) and resolution of the acquired tomographic projections [1]. We used the in-house developed high-speed CMOS GigaFRoST detector coupled to visible-light optics of $10\times$ magnification and a $20\,\mu m$ thick LuAG:Ce scintillator leading to an effective pixel size of $1.1\,\mu m$. Tomographic scans were acquired with 1501 projections of 5 ms exposure time. Including dark and flat field images, the total scan time per volume was approximately 40 seconds. Balb-C mice were first anesthetized with a mixture of Medetomidin, Midazolam and Fentanyl and an endotracheal cannula was installed after tracheotomy. The animal was placed in an upright position into a custom-made sample holder. A small-animal ventilator (SCIREQ FlexiVent) was employed for ventilation and to maintain the internal lung pressure, while acquiring the tomographic scan. Animals were sacrificied by an overdose of anaesthesia and images were taken no longer than 20 minutes afterwards to preserve *quasi-in-vivo* conditions. All animal experiments were approved and supervised by the Veterinary Service of the Cantons Aargau and Bern. Propagation-based phase-contrast was employed in order to increase the CNR of our individual projections. A single-distance phase retrieval algorithm by Moosmann *et al.* [2] was applied to every X-ray projection image and subsequently CT-reconstructed with the *gridrec* algorithm [3].

2.2. Segmentation

Since the data are acquired in interior/local tomography of a whole animal, the differentiation between air and tissue in the reconstructions varies from region to region of the volume and a gradient artifact also appears slice-wise, with tissues appearing darker on the one side of the image than the other. In addition, single-distance phase retrieval with no boundary conditions results in a super-imposed low frequency noise on the reconstructions [4]. The $5-10\,\mu m$ thick interairspace walls (alveolar septa) can be barely distinguished from the surrounding air on the basis of the grey level. An approach combining the random walk segmentation [5], a vesselness filter [6], local thresholding, and morphological closing based on the 2D average size in pixels of single alveoli has been implemented both in Python and MATLAB, and has been applied to the 8 bit depth reconstructed volume under study. The segmentation procedure can be summarized in the following steps:

Step 1) Otsu [7] thresholding results in figure (b), which is used as a basis to determine the segmentation seeds.

Step 2) 2D Connected component analysis [8] and separation between regions above and below 400 pixels (size of small alveoli with low contrast) yields images (c) and (d) respectively.

Step 3) Independent local thresholding is applied to each small local connected component (c) separately. The rest of the connected components are eroded and then combined with the locally thresholded ones, resulting in different seeds for different airspace regions, as seen in figure (d).

Step 4) A low-pass filtered images is subtracted from the raw data to enhance the edges. A 2D vesselness filter is then applied twice to obtain a single seed for all the septa resulting in the binary image of figure (e).

Step 5) Combine images (d) and (e) into a single image (f) to create the input image for the random walk.

Step 6) Random walker segmentation using the previously computed seeds as input to classify the remaining undetermined pixels. The final result can be seen in (g).

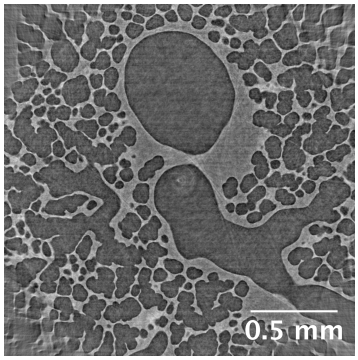

(a) Reconstructed slice

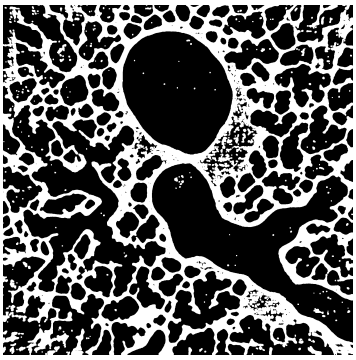

(b) Otsu thresholded slice

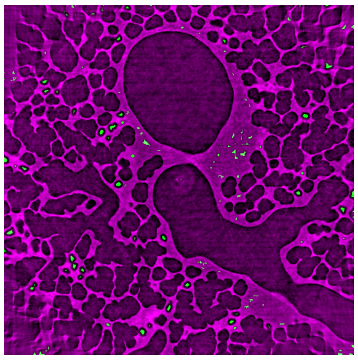

(c) Locally thresholded areas

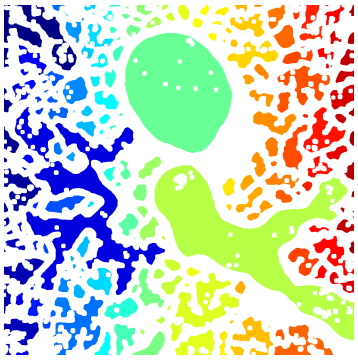

(d) Seeds for airspace

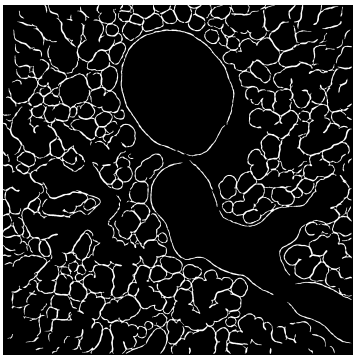

(e) Seed for the thin septa

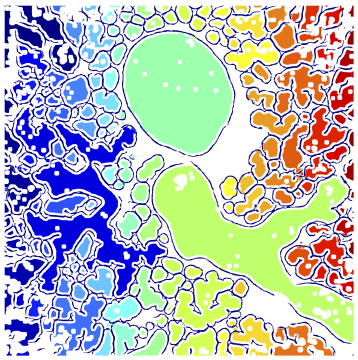

(f) Random walk input

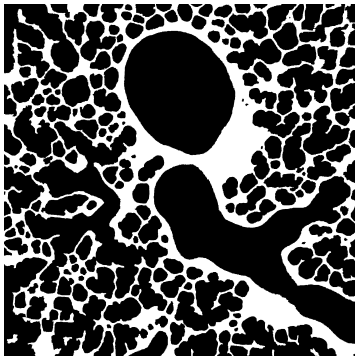

(g) Final result

Figure 1: Multilevel segmentation process. The bright pixels in (a) represent tissue and the dark ones airspace. Different colors represent different seeds with different ID (numbering). The seeds for the thin septa in (e) are all given the same ID along the whole volume. By running the final step in 3D, in a predefined number of adjacent slices, we are essentially mimicking the morphological decision done by eye whether unassigned pixels should be assigned to air or tissue i.e. by scrolling through adjacent slices.

3. Results and Discussion

In this work, we propose a novel methodology to segment 3D microstructures of fresh *post-mortem* murine lung tissue imaged inside the closed thorax. Our goal was to develop a methodology that does not require manual input or supervision. The proposed multi-level filtering approach allows us to accurately recognise lung parenchyma, despite its structural

complexity, the low CNR and the presence of local tomography and phase retrieval artifacts. Using standard thresholding methods, the thin septa, as can be seen in the top middle and bottom left of figure (b) are wrongly segmented because of low CNR, and their size being close to the resolution limit of the setup. In the final result in figure (g), they are now correctly classified as tissue by taking into account the 3D local structure of the datasets. The large septa regions that suffer from local tomography artifacts and can be seen in the middle of figure (b) are also correctly segmented. The proposed segmentation was tested on full volumes and different samples. Our method does not require any preprocessing with filters for noise removal, which is necessary for many other segmentation methods. The structural complexity of the lung parenchyma is very high and any such approach would result in altering the shape of the thin alveolar septa. Watershed based segmentation always leads to over-segmentation, due to local tomography artifacts (speckles), structural complexity and phase retrieval artifacts. Approaches, that are based on histogram models also lead to inaccurate results due to their inability of taking into account the complex structural shape of the lung parenchyma. With the proposed method, both the small and large features of the lung parenchyma are correctly segmented as seen by human eye comparison. Validation and comparison to classical histology is not straightforward due to the different thickness of the sliced sections to the tomographic slices, and also because histological sample preparation alters the microstructural thickness in a non uniform way. An automatic approach for quantifying the general improvement of the algorithm would be to simulate the whole imaging pipeline. This, however, requires apriori knowledge of the full noise model of the setup. Finally, an artificial phantom that resembles the lung parenchyma is very difficult to create due to the structural complexity of the lung and it has been a subject of research. To the best of our knowledge, no such model exists at the moment that can include multiple acini and airways into the resulting computer generated phantom.

4. Conclusion

The proposed framework provides reliable 3D segmentations of the lung microstructure, that can be used as input for any subsequent morphological analysis/quantification of the lungs at micrometer scale. In particular the described segmentation of the alveolar septa may be applied as basis for the segmentation of individual acini. An easy and reliable segmentation of the acini bears the potential for many new insights into lung function and development which are thus far hindered by the inability of classical histology to recognize individual acini. Finally, our method is also applicable in samples where feature sizes vary by more than one order of magnitude within the tomographic slices.

Acknowledgments

We would like to acknowledge Dr. Christian M. Schlepütz for his support at the TOMCAT beamline and for carefully reading the manuscript. We are thankful for the grants 310030-153468 and CR23I2-135550 of the Swiss National Science Foundation.

References

[1] Lovric G, Barré S F, Schittny J C, Roth-Kleiner M, Stampanoni M and Mokso R 2013 *Journal of applied crystallography* **46** 856–860
[2] Moosmann J, Hofmann R and Baumbach T 2011 *Optics express* **19** 12066–73
[3] Marone F and Stampanoni M 2012 *Journal of synchrotron radiation* **19** 1029–37
[4] Huang L, Zuo C, Idir M, Qu W and Asundi A 2015 *Optics letters* **40** 1976–79
[5] Grady L 2006 *IEEE transactions on pattern analysis and machine intelligence* **28** 1768–83
[6] Frangi A F, Niessen W J, Vincken K L and Viergever M A 1998 *International Conference on Medical Image Computing and Computer-Assisted Intervention* (Springer) pp 130–37
[7] Otsu N 1975 *Automatica* **11** 23–27
[8] Samet H and Tamminen M 1988 *IEEE Transactions on Pattern Analysis and Machine Intelligence* **10** 579–586